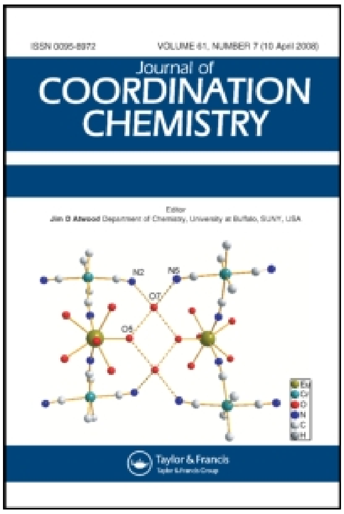

Journal of Coordination Chemistry
Publication details, including instructions for authors and subscription information:
http://www.informaworld.com/smpp/title~content=t713455674

Electrochemical properties of Hdpmta and synthesis, crystal structure as well as characterizations of a new 1D lead complex [Pb(μ_2-dpmta)$_2$(H$_2$O)$_2$]<i>_n

Yuting Wang[ab]; Zhenning Yan[a]; Yipeng Guo[a]; Yaoting Fan[a]
[a] Department of Chemistry, Zhengzhou University, Zhengzhou, Henan 450052, P.R. China [b] Department of Chemistry, Henan Institute of Education, Zhengzhou, Henan 450014, P.R. China

First published on: 22 September 2010

Journal of Coordination Chemistry
Vol. 61, No. 2, 20 January 2008, 302–313

Taylor & Francis
Taylor & Francis Group

Electrochemical properties of Hdpmta and synthesis, crystal structure as well as characterizations of a new 1D lead complex $[Pb(\mu_2\text{-dpmta})_2(H_2O)_2]_n$

YUTING WANG†‡, ZHENNING YAN*†, YIPENG GUO† and YAOTING FAN†

†Department of Chemistry, Zhengzhou University, Zhengzhou, Henan 450052, P.R. China
‡Department of Chemistry, Henan Institute of Education, Zhengzhou, Henan 450014, P.R. China

(*Received 23 November 2006; revised 31 January 2007; in final form 1 February 2007*)

A pyrimidine derivative, [(4,6-dimethyl-2-pyrimidinyl)thio] acetic acid (Hdpmta) has been synthesized and used as an ionophore in a Pb^{2+}-selective electrode. The electrode works well over a wide range of concentration (1.0×10^{-5} to $1.0 \times 10^{-2}\ \mathrm{mol\,L^{-1}}$) with the response slope of $27.4\ \mathrm{mV\,decade^{-1}}$. The electrochemical behavior of Hdpmta on glassy carbon electrode shows that in $0.1\ \mathrm{mol\,L^{-1}}$ TBAP/DMF solution, it has a well-defined irreversible cathodic peak at -0.83 V. The electrode process involves single electron transfer. Furthermore, a novel Pb(II) complex, $[Pb(\mu_2\text{-dpmta})_2(H_2O)_2]_n$ (**1**), has been synthesized through self-assembly of $Pb(OAc)_2$ with Hdpmta in aqueous solution and characterized by elemental analysis and IR spectra. X-ray diffraction analysis shows that **1** is a 1D chain structure consisting of two kinds of rhomboidal Pb_2O_2 rings, in which a large amount of H-bonding is involved. By π–π interactions parallel chains are further assembled to a 2D supramolecular network. The UV, TG and photoluminescence properties of **1** have also been investigated.

Keywords: [(4,6-Dimethyl-2-pyrimidinyl)thio] acetic acid; Electrochemistry; Ion-selective electrode; Crystal structure; Photoluminescence property

1. Introduction

Pyrimidine and its derivatives are of considerable interest because they possess excellent biological activities and pharmaceutical properties. They are an important constituent of nuclei acid, which controls the biosynthesis of proteins [1–3]. Pyrimidine moieties have favorable antibacterial, antifungal and anti-HIV activities [4–7]. Research on bioinorganic chemistry revealed that metal ions have great influence on most

*Corresponding author. Email: yanzzn@zzu.edu.cn

Journal of Coordination Chemistry
ISSN 0095-8972 print/ISSN 1029-0389 online © 2008 Taylor & Francis
DOI: 10.1080/00958970701329209

biological processes. For example, it is well known that lead can interact with biomolecules and is a major health concern. Its toxic effects originate from its multipotent involvement in interactions with enzymes and nucleic acids, where inhibition of biochemical pathways often constitutes the source of symptomatic physiological aberrations [8, 9]. The consequences of lead's interactions with biomolecules have often been ascribed to its chemistry as a borderline soft–hard metal ion [9]. For these reasons, lead complexes with pyrimidine and its derivatives have recently attracted attention. Better understanding of interactions of lead ion with pyrimidine and its derivatives will contribute to comprehending behaviors of pyrimidine compounds in biological and physiological processes.

In this work, we synthesized the ligand [(4,6-dimethyl-2-pyrimidinyl)thio] acetic acid (Hdpmta) [10]. Hdpmta is a pyrimidine derivative containing sulfide and carboxylate, which make it have not only better bioactivity [11] but also strong coordination ability. Pb(II) reacts effectively with carboxylic acids; Pb(II)-carboxylate complexes such as $Pb(C_2H_3O_2)_2 \cdot 3H_2O$ [12] and $[Pb(FcCOO)_3(bpe)]_n$ (bpe = 1,2-*bis*(4-pyridyl)ethene) [13] have been crystallographically characterized with a multitude of ligand coordination modes exhibited. By reacting Hdpmta with $Pb(OAc)_2$ in aqueous solution, a coordination polymer $[Pb(\mu_2\text{-dpmta})_2(H_2O)_2]_n$ has been obtained. The photoluminescence and TG properties of the coordination polymer and the electrochemical properties of Hdpmta have also been investigated. Furthermore, Hdpmta can be used as an ionophore for the development of PVC membrane selective electrode. The Hdpmta-based electrode using *bis*(2-ethylhexyl) sebacate (DOS) as a plasticizer exhibits near-Nernstian response characteristics towards Pb(II).

Study of the interaction of Hdpmta with Pb(II) not only helps us better understand the possible biological process of pyrimidine and Pb(II), but also provides a promising application of this ligand.

2. Experimental

2.1. *General information and materials*

All the reagents for syntheses were commercially available and employed without further purification. The Hdpmta ligand was prepared according to an improved method described in the literature [10].

Elemental analyses (C, H, N, S) were performed on a Flash EA1120 elemental analyzer. IR spectra were recorded in the region 4000–400 cm^{-1} on a Nicolet NEXUS 470-FTIR spectrophotometer with pressed KBr pellets. Emission spectra were recorded on a F-4500 HITACHI fluorescence spectrophotometer. Thermogravimetric analysis was carried out with a NETZSCH STA 409 unit at a heating rate of $10^{\circ}C\,min^{-1}$ under an argon atmosphere.

2.2. *Cyclic voltammetry*

Electrochemical experiments were performed in dry DMF using a CHI 650A electrochemical workstation. A three-electrode configuration was used. The working electrode was a GC disk (diameter 4.0 mm). The reference electrode was a saturated calomel electrode (SCE) and the auxiliary electrode was a platinum plate. The experiments were carried out under a moisture free N_2 atmosphere using $(n\text{-Bu})_4NClO_4$ (TBAP) as the supporting electrolyte.

2.3. *Potentiometric studies*

The membranes were prepared by dissolving 1.6 wt.% ionophore, 65.3 wt.% *bis*(2-ethylhexyl) sebacate (DOS), 32.7 wt.% poly(vinylchloride) (PVC) and 0.4 wt.% tetrakis(4-chlorophenyl) borate (KTpClPB) in distilled tetrahydrofuran (THF) and casting the solution in a glass ring resting on a sheet of plate glass.

Slow evaporation was achieved by weighting down a pad of filter papers on top of the ring. Discs 8 mm in diameter were cut from these master membranes and sealed onto the end of the Ag/AgCl electrode barrel with a 5 wt.% solution of PVC in THF. An internal solution of 0.001 mol L^{-1} $PbCl_2$ was used. Prior to potentiometric measurements, the electrodes were conditioned in a 0.01 mol L^{-1} sample solution overnight. The potentiometric measurements were made with the following electrochemical cell:

Hg/Hg_2Cl_2/KCl (saturated)/0.1 mol L^{-1} LiAc/sample solution//PVC membrane// 0.001 mol L^{-1} $PbCl_2$/Ag/AgCl.

Potentials were measured by using an ion meter model pXS-215 (Leici Instruments Corporation, ShangHai). The limit of detection was calculated according to the IUPAC recommendations [14]. The potentiometric selectivities were determined by a fixed interferent method, where the concentration of the primary ion was varied while those of the interference ions were 1.0×10^{-3} mol L^{-1} except Hg^{2+}, which was determined by separate solution method.

2.4. *Preparation of [Pb(μ$_2$-dpmta)$_2$(H$_2$O)$_2$]$_n$ (1)*

Hdpmta (0.0990 g, 0.5 mmol) was added to warm water (4 mL) and the resulting solution was adjusted to pH 7.0 by a 0.50 M NaOH aqueous solution. A solution of $Pb(OAc)_2 \cdot 3H_2O$ (0.0949 g, 0.25 mol) in water (4 mL) was slowly added to the above solution, and the mixture was stirred for 30 min and filtered. After one week, colorless, block-like single crystals of **1** separated from the mother liquor by slow evaporation at room temperature. The yield of **1** is ca 33% based on Hdpmta. Anal. Calcd (%) for $C_{16}H_{22}PbN_4O_6S_2$: C, 30.11; H, 3.45; N, 8.78; S, 10.04. Found: C, 30.01; H, 3.37; N, 8.86; S, 10.09. IR data (KBr, cm^{-1}): 3396(vs), 2922(m), 1662(w), 1583(s), 1552(s), 1438(w), 1424(s) 1392(s), 1340(m), 1269(vs), 1217(m), 1031(w), 930(w), 883(m), 787(w), 689(w).

2.5. *Determination of crystal structure*

A colorless single crystal of **1** with approximate dimensions $0.20 \times 0.18 \times 0.17\ mm^3$ was mounted on a glass fiber and used for data collection. All intensity data were collected on a Rigaku RAXIS-IV imaging plate area detector using graphite-monochromated Mo-Kα radiation ($\lambda = 0.71073$ Å) at room temperature to a maximum 2θ value of 50°. The unit cell parameters were determined from reflections collected on oscillation frames and were then refined. The data were corrected for Lorentz and polarization effects. The structure was solved by direct methods with the *SHELXL*-97 program [15] and subsequent Fourier-squares method on F^2 with *SHELXL*-97 [16]. The non-hydrogen atoms were refined anisotropically; hydrogen atoms were included but not refined. The final cycle of full-matrix least-squares refinement was based on the observed reflections and variable parameters. The crystallographic and refinement details are listed in table 3 and selected bond lengths and angles are listed in table 4. Full atomic data are available as a file in CIF format.

3. Results and discussion

3.1. *Redox properties of Hdpmta*

The redox behavior of the ligand has been investigated by cyclic voltammetry. Figure 1 illustrates cyclic voltammograms of Hdpmta (5.0×10^{-4} mol L^{-1}) in DMF solution recorded at several scan rates. A well-defined cathodic peak for Hdmpta in solution was observed. With increase of the scan rate (ν), cathodic peaks (E_P) shifted toward more positive potentials. No anodic peaks appear over the potential range −0.40 to −1.20 V. This behavior corresponds to a thermodynamically irreversible system. In addition it was observed that in the scan range (from 40 to 300 mV s^{-1}), peak current (i_p) is linearly proportional to scan rate (ν) (figure 1), indicating that the electrochemical process was

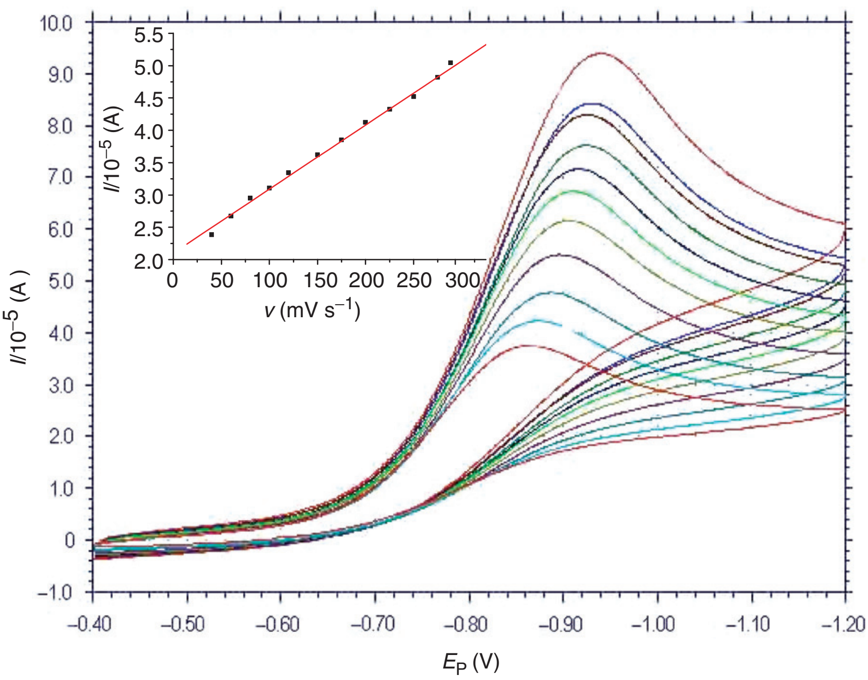

Figure 1. Cyclic voltammograms of Hdpmta at different scan rates, $\nu = 40$, 60, 80, 120, 150, 175, 200, 225, 250, 275, 300 m V s^{-1}.

controlled by adsorption. The adsorption process can be expressed by the Langmuir equation:

$$i_p = \frac{n^2F^2Av\Gamma_T}{4RT} = \frac{nFQv}{4RT} \tag{1}$$

where $Q = nFA\Gamma_T$ is the area of the peak at a definite sweep rate in a cyclic voltammetry process, Γ_T is the surface coverage, F is the Faraday constant, and A is the area of the electrode. The number of electrons transferred, n, can be calculated using equation (1). It can be seen from table 1 that Hdpmta undergoes a one-electron transfer process.

The apparent rate constant (k_S) can be calculated by Laviron's equation [17, 18]:

$$E_p = E^0 + \left[\left(\frac{RT}{\alpha nF}\right)\ln\left(\frac{RTk_S}{\alpha nF}\right) - \left(\frac{RT}{\alpha nF}\right)\right]\ln v \tag{2}$$

where α is the transfer coefficient and E^0 the formal potential. According to equation (2), the plot of E_P *versus* $\ln v$ should be linear. The slope, obtained from figure 2, was then utilized to calculate the transfer coefficient α, which is 0.74 in this study. The value of E^0 in equation (2) can be determined from intercept of E_P *versus* v plot on the ordinate by extrapolating the line to $v = 0$. The value of E^0 is -0.82 V. From the intercept of the plot in figure 2 and E^0 value, the apparent rate constant k_S was then calculated as $3.73\ s^{-1}$.

Table 1. Electron-transfer number for Hdpmta in reduction.

v ($V\,s^{-1}$)	I(A)	Q(C)	n
0.04	2.384×10^{-5}	6.579×10^{-5}	0.91
0.08	2.950×10^{-5}	4.131×10^{-5}	0.91
0.1	3.106×10^{-5}	3.568×10^{-5}	0.89
0.15	3.624×10^{-5}	2.742×10^{-5}	0.91
0.2	4.124×10^{-5}	2.402×10^{-5}	0.90

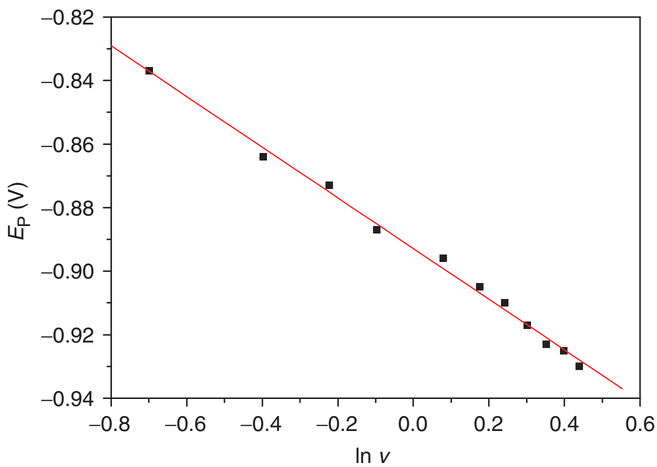

Figure 2. The relationship between E_P and $\ln v$.

Table 2. Selectivity coefficients ($\log K^{pot}_{Pb,M}$) of various interfering ions (M^{2+}).

Interfering ions	Na^+	K^+	Mg^{2+}	Ca^{2+}	Sr^{2+}	Ba^{2+}	Co^{2+}	Ni^{2+}	Cd^{2+}	Zn^{2+}	Cu^{2+}	Ag^+	Hg^{2+}
$\log K^{pot}_{Pb,M}$	−2.0	−2.2	−4.1	−2.7	−3.0	−2.8	−2.7	−2.4	−1.9	−2.9	−1.9	−1.5	2.6

3.2. *Electrode response studies*

The ligand was used as a potential neutral ionophore for preparation of a membrane of electrode for a variety of different metal ions. Among different cations examined, Pb^{2+} with the most sensitive response seems to be suitably determined with the membrane electrode. The response slope is $27.4\,mV\,decade^{-1}$ over a wide range of concentration (1.0×10^{-5} to $1.0 \times 10^{-2}\,mol\,L^{-1}$). The detection limit was $2.2 \times 10^{-6}\,mol\,L^{-1}$.

The selectivity coefficients $K^{pot}_{Pb,M}$ are shown in table 2. As can be seen from table 2, the polymer membrane containing Hdpmta as ionophore gave good $\log K^{pot}_{Pb,M}$ values against most of the interfering cations examined (i.e. Na^+, K^+, Ca^{2+}, Mg^{2+}, Sr^{2+}, Ba^{2+}, Co^{2+}, Ni^{2+}, Zn^{2+}, Cd^{2+}, Ag^+) except for Hg^{2+}, transition metal ions Co^{2+}, Ni^{2+}, Cd^{2+}, Mn^{2+}, Zn^{2+}, Cu^{2+}, Ag^+ and Hg^{2+} are reported to be serious interferences of lead ion-selective electrodes based on solid-state membranes [19, 20] and those based on a variety of different neutral ionophores [21–24]. In comparison with commercial solid-state membranes and some neutral ionophore membrane electrodes, the developed electrode in this work demonstrates the advantage of virtually no interference from transition metal ions, such as Co^{2+}, Ni^{2+}, Cd^{2+}, Zn^{2+}, Cu^{2+} and Ag^+ ions.

The response times of the PVC membrane was 20s. The electrode lifetime was about 2 weeks.

3.3. *Synthesis and crystal structure of 1*

Compound **1** was obtained as a neutral molecular complex in water by combination of Hdpmta with $Pb(OAc)_2$. Compound **1** could also be isolated using the same synthetic procedure using $Pb(NO_3)_2$ or $PbCl_2$ as the source of metal (confirmed by X-ray diffraction and IR spectra), indicating the final product is independent of the counter-anion of the metal salt. Moreover, **1** is stable in air and not soluble in common organic solvents, such as MeOH, EtOH and THF, but soluble in highly-polar solvents DMSO and DMF.

In the IR spectra of **1**, the absorption bands resulting from the skeletal vibrations of the pyrimidine ring appear at 1400–1600 cm^{-1} [25]. The broad band at 3396 cm^{-1} and weak band at 1662 cm^{-1} represent water stretching and bending vibrations, respectively, indicating the presence of coordinated water. The absence of the expected absorption at 1724 cm^{-1} for the protonated carboxylate illustrates deprotonation of the ligand in the reaction with lead. The strong absorption bands at 1552 and 1424 cm^{-1} correspond to the asymmetric and symmetrical stretching vibrations, $\nu_{as}(COO^-)$ and $\nu_s(COO^-)$ of the coordinated carboxylate group of dpmta. The weak peak at 689 cm^{-1} is assigned to the vibration of ν(C–S) [26].

Single-crystal X-ray diffraction analysis reveals that **1** is a one-dimensional chain structural polymer constructed by the basic repeating unit $[Pb(dpmta)_2(H_2O)_2]$ and the relevant crystallographic data for 1 is in table 3. As shown in figure 3, each Pb(II) is eight-coordinate with six oxygen atoms from four dpmta molecules and two oxygen

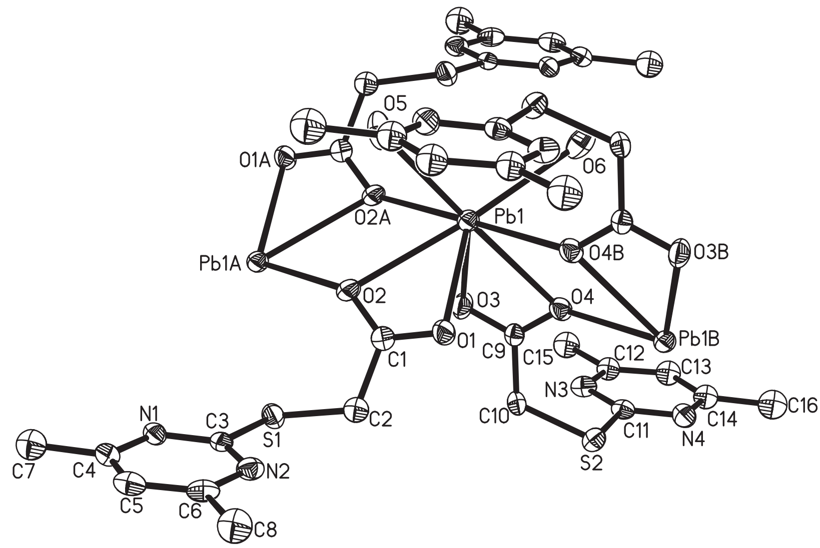

Figure 3. The asymmetric unit representation of **1** showing the local geometry around the metal center and ligand. Thermal ellipsoids were drawn at the 30% probability level.

Table 3. Crystallographic data for **1**.

Chemical formula	$C_{16}H_{22}PbN_4O_6S_2$
Formula weight	637.69
Crystal system	Triclinic
Space group	$P\bar{1}$
a (Å)	8.6394(17)
b (Å)	11.054(2)
c (Å)	12.122(2)
α (°)	71.84(3)
β (°)	86.06(3)
γ (°)	83.20(3)
V (Å^3)	1091.6(4)
Z	2
D_c (g cm^{-3})	1.940
Absorption coefficient (mm^{-1})	7.958
$F(000)$	616
θ range for data collection (°)	1.77–25.00
Index ranges	$-10 \le h \le 9$, $-13 \le k \le 0$, $-14 \le l \le 13$
Reflections collected/unique	3469/3469
Data/restraints/parameters	3469/6/235
Goodness-of-fit on F^2	1.064
Final R indices [$I > 2\sigma(I)$]	$R_1 = 0.0341$, $wR_2 = 0.0837$
R indices (all data)	$R_1 = 0.0366$, $wR_2 = 0.0848$
$\Delta\rho_{max}$, $\Delta\rho_{min}$ (e Å^{-3})	1.052, −1.517

$R_1 = \Sigma||F_o| - |F_c||/\Sigma|F_o|$; $wR_2 = [\Sigma w(F_o^2 - F_c^2)^2/\Sigma w(F_o^2)^2]^{1/2}$.

atoms from two aqua ligands. The coordination geometry around Pb can be described as a distorted bicapped anti-trigonal prism, in which two trigonal bases are defined by O6, O4, O4B($-x+2$, $-y+1$, $-z$), and O5, O2, O2A($-x+1$, $-y+1$, $-z$), and the cap positions are taken up by O1, O3 (figure 4). The dihedral angle between the triangular

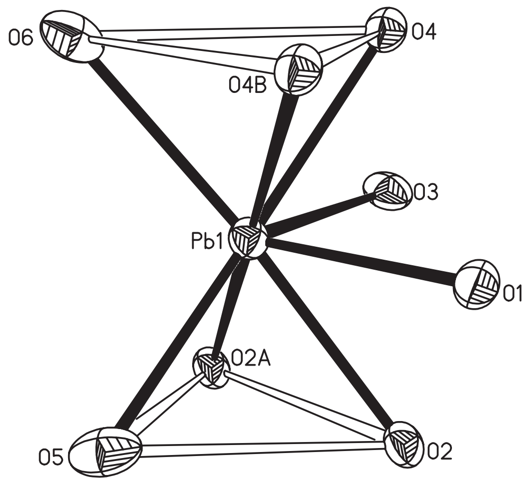

Figure 4. Coordination polyhedron of lead in **1**.

Table 4. Selected bond lengths (Å) and angles (°) for **1**.

Pb(1)–O(1)	2.552(5)	Pb(1)–O(3)	2.568(5)	Pb(1)–O(4)#1	2.614(5)
Pb(1)–O(2)#2	2.712(5)	Pb(1)–O(5)	2.766(7)	Pb(1)–O(2)	2.810(5)
Pb(1)–O(4)	2.830(5)	Pb(1)–O(6)	2.871(7)		
O(1)–Pb(1)–O(3)	74.17(19)	O(1)–Pb(1)–O(4)#1	70.64(15)	O(3)–Pb(1)–O(4)#1	108.08(16)
O(1)–Pb(1)–O(2)#2	109.82(15)	O(3)–Pb(1)–O(2)#2	68.77(15)	O(4)#1–Pb(1)–O(2)#2	176.25(15)
O(1)–Pb(1)–O(5)	103.35(19)	O(3)–Pb(1)–O(5)	136.94(16)	O(4)#1–Pb(1)–O(5)	111.39(16)
O(2)#2–Pb(1)–O(5)	72.24(16)	O(1)–Pb(1)–O(2)	48.14(15)	O(3)–Pb(1)–O(2)	74.90(16)
O(4)#1–Pb(1)–O(2)	116.07(15)	O(2)#2–Pb(1)–O(2)	65.51(17)	O(5)–Pb(1)–O(2)	72.89(17)
O(1)–Pb(1)–O(4)	74.81(16)	O(3)–Pb(1)–O(4)	47.54(15)	O(4)#1–Pb(1)–O(4)	63.49(19)
O(2)#2–Pb(1)–O(4)	112.89(15)	O(5)–Pb(1)–O(4)	174.86(15)	O(2)–Pb(1)–O(4)	108.48(14)
O(1)–Pb(1)–O(6)	137.10(16)	O(3)–Pb(1)–O(6)	105.60(18)	O(4)#1–Pb(1)–O(6)	68.89(16)
O(2)#2–Pb(1)–O(6)	109.65(16)	O(5)–Pb(1)–O(6)	104.04(19)	O(2)–Pb(1)–O(6)	174.76(14)
O(4)–Pb(1)–O(6)	74.96(16)				

Symmetry transformations used to generate equivalent atoms: #1: $-x+2, -y+1, -z$; #2: $-x+1, -y+1, -z$.

bases is 5.1°. The bond distances, Pb–O4(2.830(5) Å), Pb–O2(2.810(5) Å) and Pb–O6(2.871(7) Å) are significantly longer than the remaining Pb–O distances, which are in the range 2.552(5)–2.766(7) Å. These distances are similar to those reported in other Pb carboxylate polymers [27, 28]. In the structure of **1**, there are two crystallographically unique ligands (table 4), both displaying the same binding mode. Each ligand coordinates to two Pb(II) atoms and the carboxylate group is chelate-bridging. The remaining N atoms and the S atom of ligand are not coordinated. The interconnection of Pb centers through bridging dpmta ligands resulted in the formation of a 1D chain structural polymer along the *a* axis, as shown in figure 5. The most important structural characteristic of this chain is that there are two kinds of rhomboidal Pb_2O_2 rings within its backbone appearing alternately. The dimensions of the two rhomboidal Pb_2O_2 rings are $2.712 \times 2.810(5)$ Å^2 and 2.614×2.830 Å^2, respectively, and the dihedral angle between the two rings is 100.3°. The associated nonbonded, transannular $Pb \cdots Pb$ distances are 4.644 and 4.632 Å, respectively, comparable to reported $Pb \cdots Pb$ distances in the structures of $\{[Pb_2(FcCOO)_4(CH_3OH)] \cdot 1.5CH_3OH \cdot H_2O\}_n$ and $\{[Pb[(CH_3)_2NC_4O_3]_2\,(H_2O)_2] \cdot H_2O\}_n$, in the range from 4.044 to 4.243 Å and 4.32 to

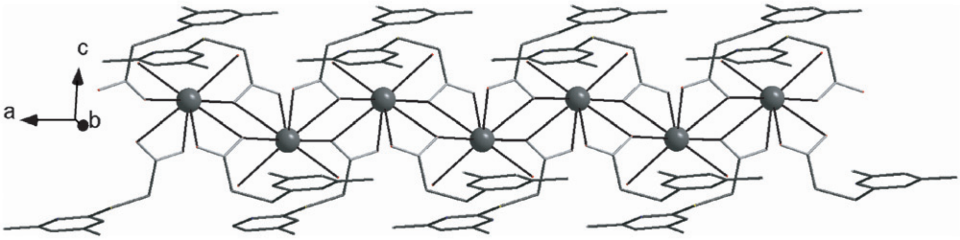

Figure 5. One-dimensional chain along *a* axis bridged by carboxylate group in **1**.

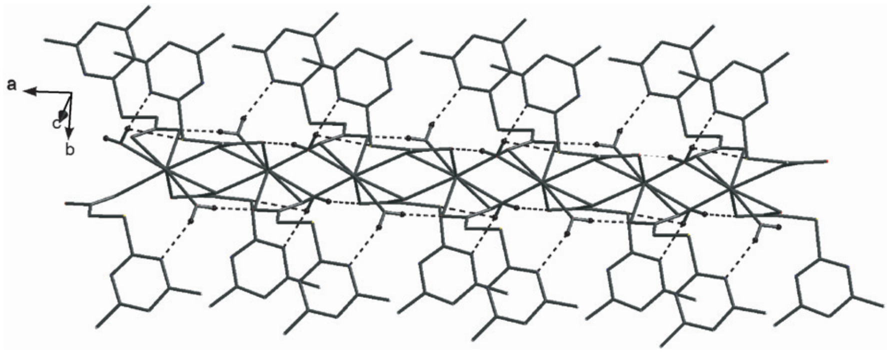

Figure 6. View of H-bonding in the 1D chain structure of **1**.

4.34 Å, respectively [28]. The vectors linking adjacent Pb atoms within the polymer chains form a zigzag with adjacent Pb $\cdots$ Pb vectors subtending an angle of 137.3°.

All ligated water molecules and dpmta ligands are involved in H-bonding interactions within the chain. Three types of H-bonding interactions are displayed in figure 6: one is between the O of coordinated water and N of pyrimidine (O5–H5E $\cdots$ N4a 2.956(9) Å, a: $-x+2$, $-y+1$, $-z$; O6–H6E $\cdots$ N1b 2.9444(8) Å, b: $-x+1$, $-y+1$, $-z$); a second arises from interaction of O of coordinated water with carboxylate O atoms (O5–H5F $\cdots$ O3b 2.735(8) Å; O6–H6F $\cdots$ O1b 2.764(8) Å); the third originates from the O of coordinated water with S of dpmta ligand (O5–H5E $\cdots$ S2a 3.282(6) Å). These intrachain hydrogen bonds stabilized the 1D polymeric structure. There are also weak π–π interactions in the extended structure of **1**. Intermolecular π–π contact occurs between pyrimidine rings belonging to neighboring parallel chains (figure S1). The distance and the dihedral angle between two pyrimidine rings are 3.379 Å and 2.28°, respectively. The centroid–centroid distance is 3.475 Å. Through π–π interactions, parallel chains further assemble into a 2D supramolecular network in the *ab* plane.

3.4. *Photoluminescence property*

The UV-vis absorption spectra of Hdpmta and **1**, determined in dilute DMF, show two absorption peaks; the peak positions and spectral shape of **1** are similar to those of Hdpmta (figure S2). The absorption spectrum of Hdpmta displays one sharp peak at 265 nm and one moderately intense absorption at 330 nm, while **1** has absorption peaks at 263 nm and 332 nm. These absorptions could be assigned to $\pi \rightarrow \pi^*$ and $n \rightarrow \pi^*$ intraligand transitions [29].

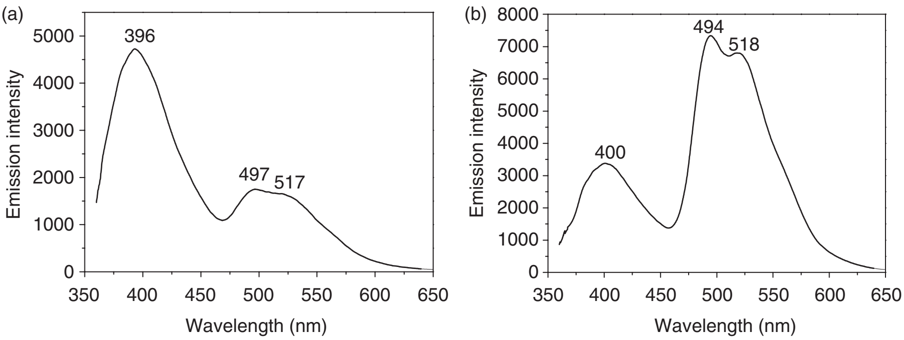

Figure 7. Solid-state emission spectra at room temperature of Hdpmta (a) and **1** (b).

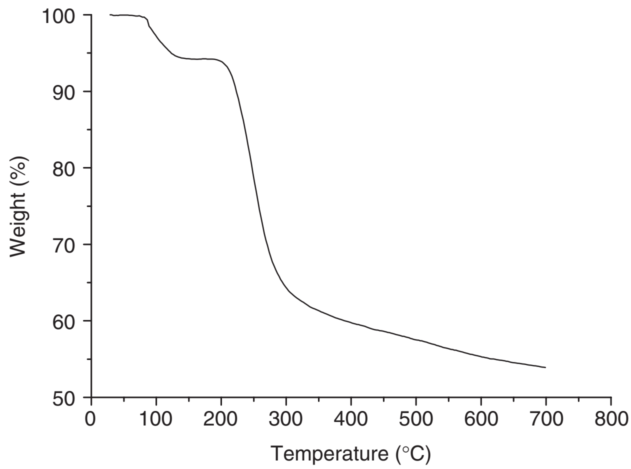

Figure 8. TGA curve of **1** under Ar atmosphere.

The luminescent emission spectra of Hdpmta and **1** in the solid state ($\lambda_{ex} = 352$ nm) at room temperature are depicted in figure 7. Hdpmta displays two intense emission peaks at 396 and 497 nm and one shoulder peak at 517 nm, attributable to different intraligand transitions of Hdpmta, such as $\pi^* \rightarrow \pi$, $\pi^* \rightarrow n$, and $n^* \rightarrow n$ transitions [30]. The emission behavior of **1** is similar to that of Hdpmta; the three emission peaks of discrete Hdpmta still appear, although these peaks are shifted a little. However, the relative intensities of the three peaks in the emission spectra of Hdpmta and **1** are different, indicating that intraligand transitions of Hdpmta have been enhanced or weakened because of the introduction of lead ion in the structure. The difference in the photoluminescence between the organic ligand and metal-organic complex is usually caused by metal involved charge transfer (i.e. LMCT) [31] but not by intraligand transitions.

3.5. *Thermogravimetric analysis*

Compound **1** is stable at ambient conditions and thermogravimetry was carried out to explore its thermal stability. TG analysis reveals that there are two main steps of decomposition in the temperature range 30–700°C (figure 8). The first step, which corresponds to the loss of two water molecules, starts about 94°C and ends at 142°C. The observed weight loss of 5.52% is in good agreement with the calculated value (5.65%). The second weight loss above 199°C is due to the decomposition of the organic moieties.

Supplementary material

Crystallographic data for **1** has been deposited at the Cambridge Crystallographic Data Center (deposition number CCDC 273548). Copies of this information can be obtained from: The Director, CCDC, 12 Union Road, Cambridge, CB2 IEZ, UK (Fax: +44 122 333 6033; Email: deposit@ccdc.cam.ac.uk; web: http://www.ccdc.cam.ac.uk). View of π–π interactions of pyrimidine rings in 1 (figure S1). UV/Vis spectra and of Hdpmta and **1** (figure S2).

Acknowledgements

This work was supported by the National Natural Science Foundation of China (No. 20471053), the China National Key Basic Research Special Funds (No. 2003CB214500) and the Energy & Technology Program from Zhengzhou University.

References

[1] J.G. Contreras, V. Seguel. *Spectrochim. Acta A*, **48**, 525 (1992).
[2] A. Pullman. *Adv. Hetrocycl. Chem.*, **13**, 77 (1971).
[3] V. Krishnakumar, R. John Xavier. *Spectrochim. Acta A*, **63**, 454 (2006).
[4] S.N. Pandeya, D. Sriram, G. Nath, E. De Clercq. *Il Farmaco*, **54**, 624 (1999).
[5] M. Johar, T. Manning, D.Y. Kunimoto, R. Kumar. *Bioorg. Med. Chem.*, **13**, 6663 (2005).
[6] A. Agarwal, K. Srivastava, S.K. Puri, S. Sinha, P.M.S. Chauhan. *Bioorg. Med. Chem. Lett.*, **15**, 5218 (2005).
[7] A. Agarwal, K. Srivastava, S.K. Puri, P.M.S. Chauhan. *Bioorg. Med. Chem. Lett.*, **13**, 6226 (2005).
[8] J. Palca. *Science*, **253**, 842 (1991).
[9] M. Kourgiantakis, M. Matzapetakis, C.P. Raptaopoulou, A. Terzis, A. Salifoglou. *Inorg. Chim. Acta*, **297**, 134 (2000).
[10] M.P.V. Boarland, J.F.W. McOmie, R.N. Timms. *J. Chem. Soc.*, 4691 (1952).
[11] A.N. Kharchuk, G.V. Protopopova, V.G. Telyuk, K.V. Fedotov, E.K. Mikitenko. *Fizio. Aktiv. Vesh.*, **20**, 21 (1988).
[12] R.G. Bryant, V.P. Chacko, M.C. Etter. *Inorg. Chem.*, **23**, 3580 (1984).
[13] H.W. Hou, L.K. Li, G. Li, Y.T. Fan, Y. Zhu. *Inorg. Chem.*, **42**, 3501 (2003).
[14] G.G. Guilbault, R.A. Durst, M.S. Frant, H. Freiser, E.H. Hansen, T.S. Light, E. Pungor, G.A. Rechnitz, N.M. Rice, T.J. Rohm, W. Simon, J.D.R. Thomas. *Pure Appl. Chem.*, **48**, 127 (1976).
[15] G.M. Sheldrick. *Acta Crystallogr., Sect. A*, **46**, 467 (1990).
[16] G.M. Sheldrick. *SHELXL-97, Program for the Refinement of Crystal Structures*, University of Göttingen, New York (1997).
[17] E. Laviron. *J. Electroanal. Chem.*, **52**, 355 (1974).
[18] E. Laviron. *J. Electroanal. Chem.*, **101**, 19 (1979).
[19] M. Mascini, A. Liberty. *Anal. Chim. Acta*, **60**, 405 (1972).
[20] D. Midgley. *Anal. Chim. Acta*, **159**, 63 (1984).

[21] S.R. Sheen, J.S. Shih. *Analyst*, **117**, 1691 (1992).
[22] S.K. Srivastava, V.K. Gupta, S. Jain. *Analyst*, **120**, 495 (1995).
[23] N. Tavakkoli, Z. Khojasteh, H. Sharghi, M. Shamsipur. *Anal. Chim. Acta*, **360**, 203 (1998).
[24] Z. Yan, Y. Hou, Z. Zhou, C. Du, Y. Wu. *Anal. Letts.*, **37**, 3149 (2004).
[25] (a) S. Akyüz, T. Akyüz. *J. Mol. Struct.*, **651–653**, 205 (2003); (b) S. Breda, I.D. Reva, L. Lapinski, M.J. Nowak, R. Fausto. *J. Mol. Struct.*, **786**, 193 (2006); (c) I.S. Butler, Y. Huang, N. Hadjiliadis. *Inorg. Chim. Acta*, **231**, 191 (1995).
[26] R.R. Shagidullin, A.V. Chernova, Z.G. Bazhanova, J.H. Lii, V.E. Kataev, S.A. Katsyuba, V.S. Reznik. *J. Mol. Struct.*, **707**, 1 (2004).
[27] (a) M. Kourgiantakis, M. Matzapetakis, C.P. Raptopoulou, A. Terzis, A. Salifoglou. *Inorg. Chim. Acta*, **297**, 134 (2000); (b) X.B. Wang, J.J. Vittal. *Inorg. Chem. Comm.*, **6**, 1074 (2003).
[28] (a) G. Li, H.W. Hou, L.L. Li, X.R. Meng, Y.T. Fan, Y. Zhu. *Inorg. Chem.*, **42**, 4995 (2003); (b) D.J. Williams, S. Menzer, A.J.P. White. *Inorg. Chem.*, **36**, 3096 (1997).
[29] (a) D.T. McQ, A.E. Pullen, M.S. Timothy. *Chem. Rev.*, **100**, 2537 (2000); (b) H.S. Joshi, R. Jamshidi, T. Yitzhak. *Angew. Chem. Int. Ed.*, **38**, 2722 (1999); (c) H.W. Hou, Y.T. Fan, C.X. Du, Y. Zhu, W.L. Wang, X.Q. Xin, M.K.M. Low, W. Ji, H.G. Ang. *Chem. Commun.*, 647 (1999).
[30] (a) X.D. Chen, M. Du, T.C.W. Mak. *Chem. Commun.*, 4417 (2005); (b) W. Chen, J.Y. Wang, C. Chen, Q. Yue, M.H. Yuan, J.X. Chen, S.N. Wang. *Inorg. Chem.*, **42**, 944 (2003).
[31] (a) L.Y. Zhang, G.F. Liu, S.L. Zheng, B.H. Ye, X.M. Zhang, X.M. Chen. *Eur. J. Inorg. Chem.*, 2965 (2003); (b) Y. Gong, W. Tang, W.B. Hou, Z.Y. Zha, C.W. Hu. *Inorg. Chem.*, **45**, 4987 (2006).